Pressure-induced collapse of ferromagnetism in nickel

A. Ahad [1,*] and M. S. Bahramy [2,†]

[1]*Department of Physics, Aligarh Muslim University, Aligarh 202002, India*

[2]*Department of Physics and Astronomy, The University of Manchester, Manchester M13 9PL, United Kingdom*

(Received 26 August 2021; revised 22 December 2021; accepted 23 December 2021; published 4 January 2022)

Transition metals Fe, Co, and Ni are the canonical systems for studying the effect of external perturbations on ferromagnetism. Among these, Ni stands out as it undergoes no structural phase transition under pressure. Here we have investigated the long-debated issue of the pressure-induced magnetization drop in Ni from first principles. Our calculations confirm an abrupt quenching of magnetization at high pressures not associated with any structural phase transition. We find that the pressure substantially enhances the crystal-field splitting of Ni-3*d* orbitals, driving the system toward a new metallic phase violating the Stoner Criterion for ferromagnetic (FM) ordering. Analyzing the charge populations in each spin channel, we show that the next-nearest-neighbor interactions play a crucial role in quenching FM ordering in Ni and materials alike.

DOI: 10.1103/PhysRevB.105.024404

I. INTRODUCTION

In transition metals such as Fe, Co, and Ni, the strong exchange interaction between the valence shell 3*d* electrons leads to itinerant ferromagnetic (FM) ordering with a sizable saturated magnetic moment M. External perturbations like pressure (P), temperature, and magnetic field enable manipulating this ordering and its underlying mechanisms. Among these stimuli, the application of P is particularly of great utility as it allows studying the interplay of spin, orbital, and lattice degrees of freedom of electron under controlled conditions [1]. Accordingly, extensive experimental and theoretical studies have already been performed to understand the collective behavior of 3*d* electrons in such cross-correlated systems.

In general, P tends to decrease the interatomic distances, thereby enhancing the overlap of the atomic wave functions [2] which itself results in band broadening and promotion of electrons to higher energy states, ultimately increasing the kinetic energy of electrons, causing delocalization [3]. More specifically speaking, broadening reduces the density of states (DOS) at the Fermi level (E_F), leading to the violation of the Stoner criterion (SC) for spontaneous magnetism [4,5], i.e., $U\mathrm{DOS}(E_F) \equiv I\mathrm{DOS}(E_F) > 1$, where U is the Hubbard parameter and I corresponds to the so-called Stoner parameter. In the case of Fe and Co, such a collapse of FM ordering occurs at ∼14 and ∼100 GPa, respectively [6,7]. On the other hand, Ni, which has a close-packed face-centered cubic (FCC) structure with a relatively small $M = 0.6\mu_B$/Ni, can survive up to extremely high Ps [3,8]. Previous *ab-initio* calculations have suggested a monotonic decrease of M in Ni for Ps up to 100 GPa [9]. Under high Ps, Ni tends to become nonmagnetic but remains metallic. High-pressure x-ray magnetic circular dichroism (XMCD) experiments also have indicated [10] a weak decrease in K-edge signal in Ni, representing its magnetization even when the volume (V) compresses by 80% (i.e., $V/V_0 = 0.8$, with V_0 being the volume at the ambient pressure). At higher compressions, the K-edge signal exhibits a more significant suppression, suggesting a phase transition to a nonmagnetic state at $P = 250$ GPa. This observation is, however, contradicted by a similar experiment [11] showing the resistance of the FM phase for volume compressions up to $V/V_0 = 0.66$ ($P = 200$ GPa). Using density functional theory (DFT) calculations, the authors of the latter work have claimed that the K-edge signal stems from the 4*p* orbital moment rather than the total spin moment and speculated that the nonmagnetic state could only occur above 400 GPa. This claim is further supported by a nuclear forward scattering experiment, demonstrating the survival of the FM phase up to 260 GPa [3].

Here we revisit this long-standing problem from a physicochemical perspective, taking into account the symmetry relations between the bonding orbitals and the local magnetic moments. Systematically analyzing the spin and orbital characters of the bonding states in Ni through first-principles calculations, we confirm the quenching of the FM ordering at high pressures and propose an *interspin* charge transfer mechanism as its driving force. The characteristic feature of this mechanism is a continuous transfer of charge from the spin majority channel to the spin minority channel caused by an enhancement of crystal-field splitting of Ni-3*d* orbitals.

II. COMPUTATIONAL METHOD

The electronic structure calculations are performed within DFT using the Perdew-Burke-Ernzerhof (PBE) exchange-correlation functional [12] and ultrasoft pseudopotential as implemented in QUANTUM ESPRESSO [13]. The FCC lattice

*Present address: Jawaharlal Nehru Centre for Advanced Scientific Research Bengaluru 560064, India; abdulahad@jncasr.ac.in

†m.saeed.bahramy@manchester.ac.uk

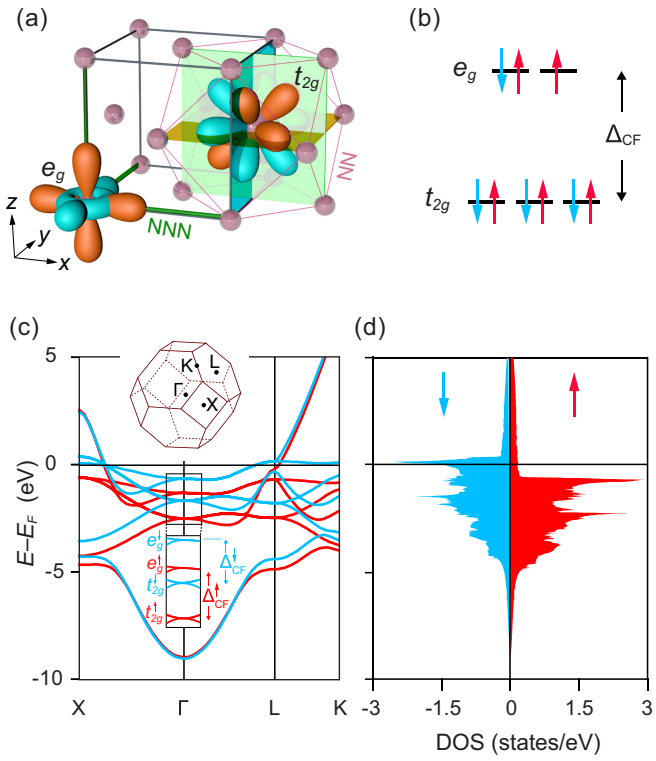

FIG. 1. Schematic illustration of (a) the crystal structure of Ni and (b) its corresponding crystal-field Δ_{CF}, experienced by the e_g and t_{2g} orbitals. Each Ni is cuboctahedrally coordinated via t_{2g} orbitals with its NNs indicated with the purple lines in (a). NNN is indicated by the thick green lines in (a). (c) and (d) The spin-resolved electronic band structure and DOS of Ni at ambient pressure, respectively. The inset in (c) is the corresponding BZ and high symmetry k points.

parameter at ambient pressure is set to $a = 3.506$ Å [14]. The body-centered cubic (BCC) and hexagonal close-pack (HCP) lattices have also been constructed to examine the structural stability of Ni in the FCC phase relative to other possible structures. For all these three phases, the effect of P is treated by optimizing the volume of Ni lattice without breaking the crystal symmetry using the Broyden-Fletcher-Goldfarb-Shanno algorithm [15]. The corresponding Brillouin zones (BZs) are sampled by a $60 \times 60 \times 60$ k mesh for FCC, a $54 \times 54 \times 54$ k mesh for BCC, and a $30 \times 30 \times 15$ k mesh for HCP using the Gaussian smearing method with a broadening energy width of 0.01 Ry. The electron hopping parameters have been deduced from a low-energy tight-binding model downfolded from the DFT Hamiltonian of the FCC structure using maximally localized Wannier functions [16,17], with Ni-3d orbitals being chosen as the projection centers.

III. RESULTS AND DISCUSSION

A. Structural and electronic properties of nickel

The conventional unit cell of Ni is shown in Fig. 1(a). This close-packed FCC structure allows each Ni to be coordinated with 12 neighbors [18,19], thereby giving the whole structure the highest possible symmetry among all space groups (Fm-$3m$). Such cuboctahedral coordination gives rise to a cubic crystal-field Δ_{CF}, splitting the Ni-3d orbitals into two subgroups e_g composed of axially oriented $\{d_{x^2-y^2}$ and $d_{z^2}\}$ orbitals and t_{2g} composed of diagonally oriented $\{d_{xz}$, d_{yz} and $d_{xy}\}$ orbitals. As each nearest neighbor (NN) of Ni is diagonally coordinated, the t_{2g} orbitals more effectively contribute to the Ni-Ni bonds [see Fig. 1(b)]. Accordingly, they tend to lie below the e_g states and show a stronger energy dispersion. As a result, the e_g states form a flat band at and in the vicinity of E_F, promoting strong e-e Coulomb interaction. The system lowers this unfavorable energy term by breaking its time-reversal symmetry, leading to an itinerant FM order. While this allows pushing the energy bands below E_F in the spin majority channel (↑), in the spin minority channel (↓) there is still a significant contribution from e_g flat bands, appearing as a sharp van Hove peak in the DOS at E_F, as shown in Figs. 1(c) and 1(d). The resulting itinerant FM phase is found to hold a nominal $3d^9$ state [20] with a net saturated magnetization of $M = 0.6$ μ_B/Ni, in good agreement with experiment [3].

B. Effect of pressure

To understand how P affects the electronic structure, we have summarized the volumetric, magnetic, and electronic properties of Ni as functions of P in Fig. 2. We have first examined the structural stability of nickel by comparing its free energy (E) in the FCC phase with that of BCC and HCP phases. As shown in Fig. 2(a), the FCC structure remains energetically more stable than the other two phases for the whole range of pressures considered in this work (P up to 1000 GPa). On the other hand, the HCP phase appears to be the least stable structure. The corresponding energy difference between the HCP and the FCC phases continuously grows with increasing P, reassuring that nickel does not prefer to be in a noncubic structure even at extremely high pressures. This finding is consistent with the previous calculations by Jarlborg [21], showing that the FM FCC phase of nickel is the most stable structure among these three phases for a wide range of pressures. We have therefore focused our attention on the FCC phase, hereafter.

As can be seen in Figs. 2(a)–2(c), E, V, and E_F respond monotonously to the increase in P. In contrast, the magnetization drops discontinuously at the critical pressure $P_c = 810$ GPa; see Fig 2(d). Particularly, the increase in E_F can be well described by Sommerfeld's power-law relation $E_F \propto P^{2/5}$, as shown in Fig. 2(b). Such a disparity in magnetic and volumetric properties of Ni under P is a strong indication of a spontaneous violation of the SC without any structural symmetry breaking. In other words, the P-induced inflation of the BZ is so strong that it can alone modify the dispersion of the energy bands, including the flat e_g bands, such that the net DOS(E_F) is no longer sufficient to satisfy the SC for FM ordering. To assure the magnetization drop is not an artifact in our DFT calculations (for example, due to trapping in a local minimum energy configuration), we have calculated the energy difference between the FM and the nonmagnetic phases of FCC nickel $\Delta E_{\text{FM-NM}} = E_{\text{FM}} - E_{\text{NM}}$ as a function of P; see Fig. 2(d). This figure clearly supports the previous finding that nickel, in general, prefers FM FCC configura-

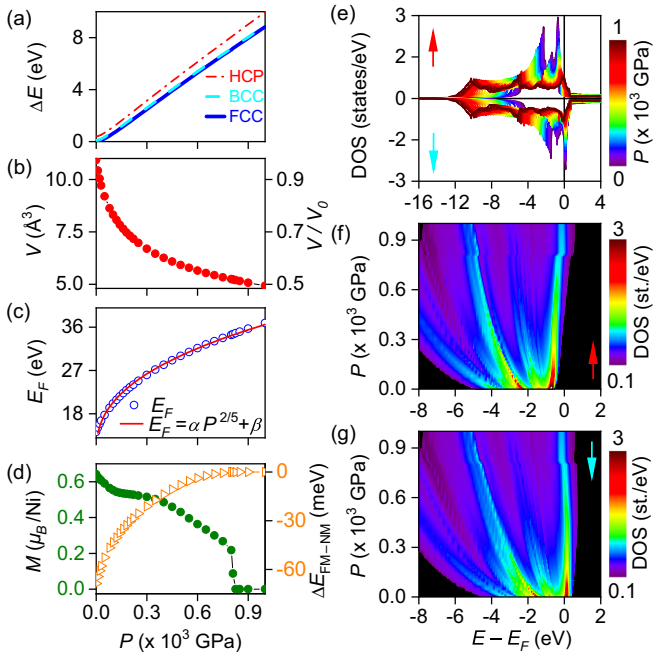

FIG. 2. (a) Calculated free energy $\Delta E(P) = E_i(P) - E_{\rm FCC}(0)$ for the i = FCC, BCC, and HCP phases of nickel as a function of pressure P. $E_{\rm FCC}(0)$ corresponds to the total energy of the FCC phase at the ambient pressure. (b)–(d) Pressure dependence of volume (V), Fermi energy (E_F), and magnetization (M) in the FCC phase, respectively. The solid line in (b) is the corresponding curve obtained from fitting the calculated results to Sommerfeld's free electron model $E_F = \alpha P^{2/5} + \beta$, with $\alpha = 6.740\,\text{meV.Pa}^{-2/5}$ and $\beta = 9.698\,\text{eV}$. Panel (d) also includes the pressure dependence of the energy difference $\Delta E_{\text{FM-NM}}(P) = E_{\rm FM}(P) - E_{\rm NM}(P)$, where $E_{\rm FM}(P)$ and $E_{\rm NM}(P)$ are the free energies of FM and nonmagnetic states of FCC nickel at pressure P, respectively. (e)–(g) Different representations of spin-resolved DOS as a function of pressure.

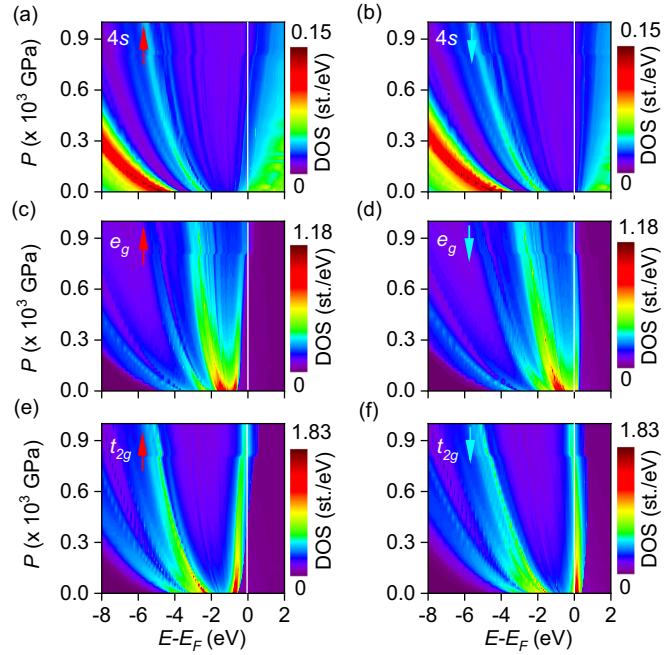

FIG. 3. Heatmap plots of spin-projected DOS resulting from (a) $4s^{\uparrow}$, (b) $4s^{\downarrow}$, (c) $e_g^{\uparrow}$, (d) $e_g^{\downarrow}$, (e) $t_{2g}^{\uparrow}$, and (f) $t_{2g}^{\downarrow}$ orbitals.

tion [21]. However, it loses its strength as P increases and eventually turns into a nonmagnetic phase $\Delta E_{\text{FM-NM}} = 0$ as P reaches P_c.

The DOS plots shown in Fig. 2(e) further support the scenario of the magnetization collapse at high Ps. This is more evident in the heatmap plots shown in Figs. 2(f) and 2(g). As can be seen, the DOS near and at E_F is abruptly perturbed at P_c. The trend of changes is, however, opposite between the two spin channels. For spin-↑ states, this appears as a sudden shift of DOS above E_F, whereas in the spin-↓ channel, DOS shifts downward, suggesting a spontaneous *interspin* charge transfer at P_c. Logically this means a redistribution of charge, partly moving the $t_{2g}^{\uparrow}$ electrons used to form the NN Ni-Ni bonds to $e_g^{\downarrow}$ orbitals to enhance the next-nearest-neighbor (NNN) Ni-Ni bonds as they become increasingly shorter under P [see Fig. 1(a)].

To examine this, we have calculated the spin- and orbital-projected DOS for a wide range of Ps; see Fig. 3. These calculations confirm that the pressure enhances the electronic dispersions of the bands throughout the whole energy spectrum and irrespective of their orbital characters. Interestingly, for 4s orbitals, this enhancement equally affects bonding and antibonding branches, causing the former (latter) to extend to lower (higher) energies; see Figs. 3(a) and 3(b). As this implies a partial depletion of 4s charges near E_F, one may expect that part of the charge transfer mentioned above comes from the 4s electrons. However, the charge provided this way is not enough to fill the unoccupied $3d^{\downarrow}$ states (compare the DOS scales in Fig. 3). Accordingly, the prime contributor for the expected band filling and its resulting magnetization collapse is a charge transfer from $t_{2g}^{\uparrow}$ and $e_g^{\uparrow}$ to their corresponding spin-↓ counterparts. This can indeed be seen in Figs. 3(c)–3(f). The most contrasting feature in these plots is a unilateral expansion of DOS toward lower energies under P. At and near E_F, the changes are minute but critical. Here one can notice a compensating behavior between the two spin channels, appearing as an upward (downward) shift of the edge of $\text{DOS}^{\uparrow}$ ($\text{DOS}^{\downarrow}$). Together with the overall enhancement of band dispersions, this leads to a substantial decrease of $\text{DOS}^{\downarrow}(E_F)$. In other words, by applying P, the previously unoccupied $t_{2g}^{\downarrow}$ and $e_g^{\downarrow}$ states increasingly gain charge from their counterparts in the other spin channel. Remarkably at P_c, a sudden charge transfer takes place, abruptly pushing all the $t_{2g}^{\downarrow}$ and $e_g^{\downarrow}$ states below E_F and quenching magnetization entirely.

To clarify this further, we have also calculated the spin- and orbital-projected band structures at three Ps (0, 810, and 1000 GPa), representing low, critical, and high Ps, respectively; see Fig. 4. As is evident, the pressure enhances the dispersion of the bands, thereby weakening the overall Coulomb interaction to the extent that the bands become nearly spin-degenerate at high Ps. The flatness of e_g bands and localization near E_F at low Ps can also be seen in this figure. Under P, they become increasingly dispersed, confirming strong electron hopping between the NNN Ni sites, as discussed earlier. One can also see a drastic enhancement of the bonding-antibonding gap of t_{2g} states at X point, followed

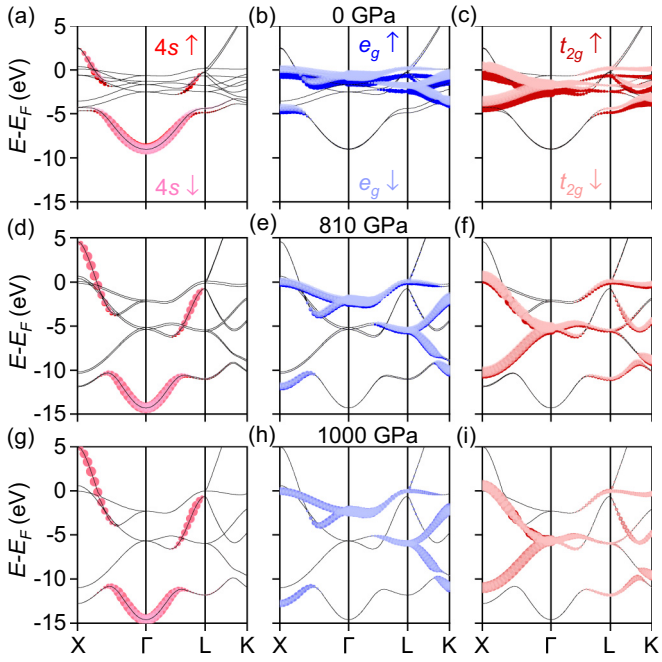

FIG. 4. Spin- and orbital-projected band structures of Ni calculated at the ambient pressure (a)–(c), the critical pressure 810 GPa (d)–(f), and 1000 GPa (g)–(i).

by a sizable downward shift of the whole t_{2g} bands, maintaining their band edge at E_F. Such profound changes in the electronic structure clearly show how pressure acts against the SC through the cubic crystal field of Ni, enabling a complete collapse of magnetization.

C. Violation of Stoner criterion

To demonstrate how P violates the SC, we show in Fig. 5(a) the P dependence of $\Delta^{\sigma}_{\mathrm{CF}}$ for both spin channels $\sigma = \uparrow$ and $\downarrow$. At low Ps, $\Delta^{\sigma}_{\mathrm{CF}}$ is found to be small and comparable to the NN magnetic exchange-coupling energy $J_{\mathrm{ex}} \simeq J_{\mathrm{NN}}$. This can be justified using a mean-field Ising model $\Delta E_{\mathrm{ex}} \simeq -J_{\mathrm{NN}} \sum_{i=\mathrm{NN}} \mathbf{S}_0 \cdot \mathbf{S}_i = -12 J_{\mathrm{NN}}$, considering an FM ordering between the 12 NNs of Ni. Within this regime, the obvious dominance of ΔE_{ex} does not allow the electrons to be delocalized, therefore substantially suppressing $\Delta^{\sigma}_{\mathrm{CF}}$. Increasing P promotes the charge transfer, as explained above, and hence monotonously enhances $\Delta^{\sigma}_{\mathrm{CF}}$ against ΔE_{ex}. Eventually it completely eliminates J_{NN} and so becomes the dominant source of band splitting. Considering that U corresponds to the spin splitting of the energy states at Γ point [see Fig. 5(a)], we can show that the criterion $U\mathrm{DOS}(E_F) > 1$ is violated once $P > P_c$; see Fig. 5(b). This is further supported by a direct calculation of the stoner parameter I using the method proposed by Bekaert *et al.* [22]; see the inset in Fig. 5(b). From this calculation, we deduce $I = 1.393$ eV, excellently confirming the validity of the Stoner condition $I\mathrm{DOS}(E_F) > 1$ for $P < P_c$ and its violation for $P > P_c$.

To provide further evidence that the magnetization collapse in Ni is due to the enhancement of Δ_{CF}, we have explicitly calculated the NN (J_{NN}) and the NNN (J_{NNN}) exchange parameters using the method proposed by Xiang *et al.* [23]. For each parameter, we have performed a set of four calculations with different collinear magnetic states: (1) $S^z_0 = S$ and $S^z_i = S$, (2) $S^z_0 = S$ and $S^z_i = -S$, (3) $S^z_0 = -S$ and $S^z_i = S$, and (4) $S^z_0 = -S$ and $S^z_i = -S$. Here i = NN or NNN, and the quantization axis is assumed to be along the z axis. For ionic sites

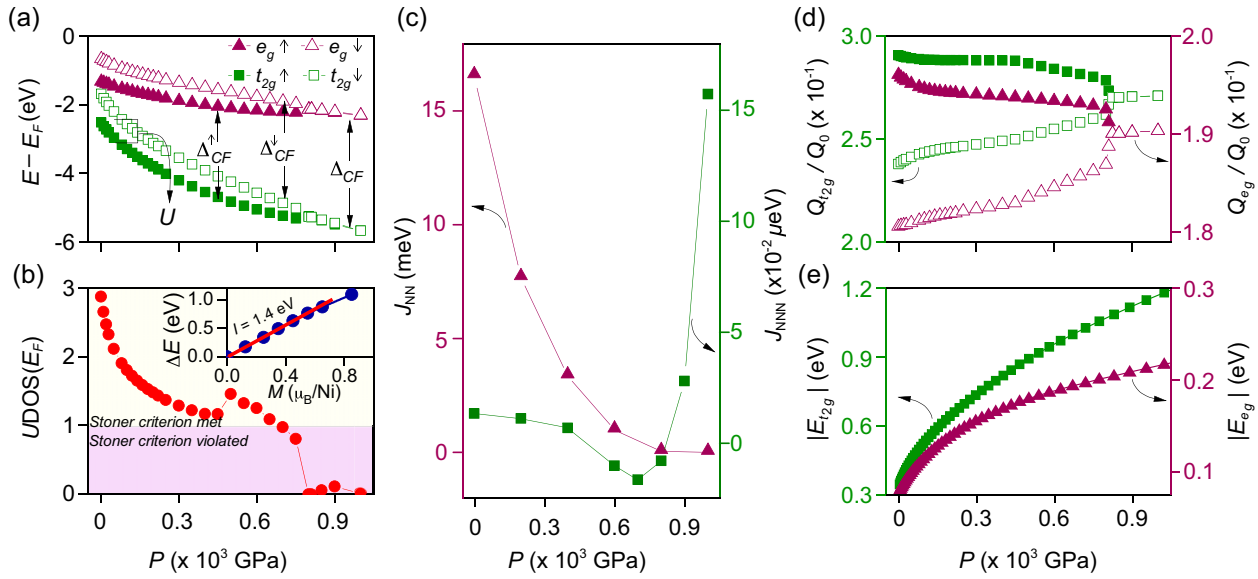

FIG. 5. (a) P dependence of the crystal-field-splitting $\Delta^{\uparrow\downarrow}_{\mathrm{CF}}$ and the magnetic exchange-splitting J_{ex} between e_g and t_{2g} states. (b) The evolution of SC as a function of P. The inset shows the variation of energy versus magnetization at the ambient pressure. Fitting the calculated results using a linear curve, we have extracted the Stoner parameter I at the ambient pressure using the method described in Ref. [22]. (c) Evolution of the NN (J_{NN}) and NNN (J_{NNN}) exchange-coupling parameters under pressure. (d) Normalized partial charges on Ni atom decomposed to $e_g^{\uparrow\downarrow}$ and $t_{2g}^{\uparrow\downarrow}$ orbitals. Q_0 corresponds to the total charge at the Fermi level at the ambient pressure. (e) Pressure dependence of NN hopping $E_{t_{2g}}$ and NNN hopping E_{e_g} between Ni ions.

other than 0 and i, we have taken the same spin orientation. After obtaining the total energy of each spin configuration, we have extracted the exchange parameter J_i using the following formula [23]

$$J_i = \frac{E_1 + E_4 - E_2 - E_3}{4S^2}, \text{ with } i = \text{NN or NNN}. \quad (1)$$

The corresponding J_{NN} and J_{NNN} are shown in Fig. 5(c) as functions of P. These calculations suggest that J_{NN} is the dominant exchange-coupling term at low pressures (i.e., $J_{\text{NN}} \gg J_{\text{NNN}}$). However, it rapidly decreases by increasing P and vanishes at and above P_c. On the other hand, J_{NNN} shows a sudden increase above P_c. However, it is not so strong to cause any magnetic ordering.

D. Interspin charge transfer mechanism

To quantify the rate and amount of charge transferred between the spin channels, we have performed Löwdin charge population analysis using partial charge densities centered at Ni sites at various Ps; see Fig. 5(d). Our calculation reveals that for Ps up to 400 GPa, the charge transfer is predominantly from $e_g^{\uparrow}$ to $e_g^{\downarrow}$ and $t_{2g}^{\downarrow}$. Within this range, the $t_{2g}^{\uparrow}$ charge, except for a minor drop at low Ps, is nearly constant. This is consistent with our previous finding that the van Hove singularities near E_F are dominated by e_g states. Beyond 400 GPa, the $t_{2g}^{\uparrow}$ population drops sharply and rapidly exceeds the $e_g^{\uparrow}$ charge drop. Consequently, the charge gained by $e_g^{\downarrow}$ and $t_{2g}^{\downarrow}$ states boosts dramatically and grows linearly. This implies that such massive compressive forces have shrunk the Ni lattice so much that its NNN Ni bonds are now as effectively involved in charge transfer as NN Ni bonds. Eventually, at P_c, the charge transferred from (to) $e_g^{\uparrow}$ and $t_{2g}^{\uparrow}$ ($e_g^{\downarrow}$ and $t_{2g}^{\downarrow}$) drops (jumps) abruptly and then remains constant. The system is now in a new equilibrium state with equal charges in both spin channels. As such, it becomes nonmagnetic and remains so for $P \geqslant P_c$.

Figure 5(e) provides a more quantitative picture of charge redistribution in Ni under pressure. Here we have shown the σ-type hopping parameters between the NN and the NNN Ni-3d orbitals using maximally localized Wannier functions. These parameters directly correspond to the NN hopping between the Ni-t_{2g} orbitals, denoted as $E_{t_{2g}}$, and the NNN hopping between the Ni-e_g orbitals, denoted as E_{e_g}. As is evident, on increasing P, both $E_{t_{2g}}$ and E_{e_g} show a monotonic increase, reconfirming that the pressure drastically enhances the interaction and charge transfer between the Ni ions through both the NN and the NNN channels.

E. Electron correlation and relativistic effects

It is worth mentioning that a previous report has suggested that the competition of electron correlation and spin-orbit coupling (SOC) may result in magnetic anisotropy in Ni [24], even though it naturally behaves as an itinerant ferromagnet [25,26]. Some also have suggested that SOC alone plays a key role in the observed magnetization drop in Ni under pressure. In general, the 3d transition metal elements are known to be capable of exhibiting strong electron correlation effects both

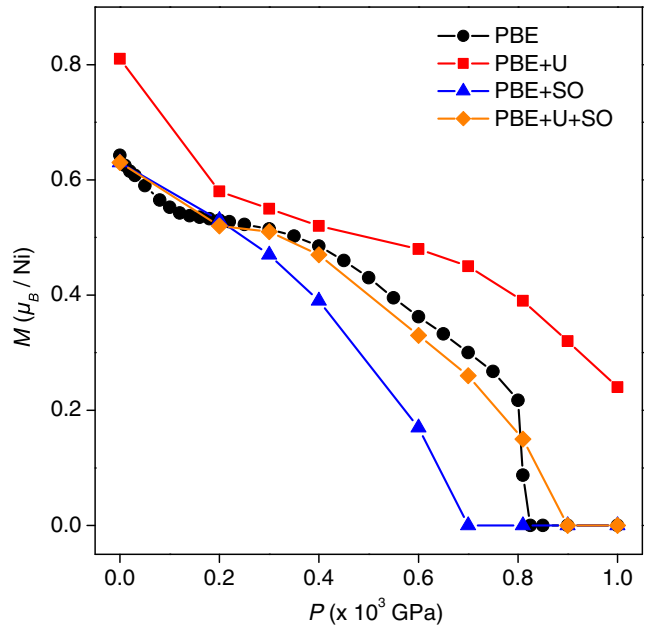

FIG. 6. P dependence of magnetization obtained using different methods.

at ambient conditions and under pressure [27–29]. To examine the contributions of both electron correlation effects and SOC, we have performed additional calculations incorporating the onsite Hubbard U and SOC corrections. As can be seen in Fig. 6, the inclusion of SOC (PBE + SOC) leads to a lower P_c. On the other hand, the incorporation of the onsite Hubbard U (PBE + U) pushes P_c far above 1000 GPa. The latter method also leads to an overestimation of M at ambient pressure. Interestingly, when both SOC and U are included (PBE + U + SOC), we see a behavior that is very much similar to that of pure PBE calculations. The most striking difference is now a milder quenching of M at a slightly higher P_c compared with that obtained by the PBE exchange-correlation functional.

IV. CONCLUSIONS

In summary, we systematically investigated the origin of magnetization quenching in the nickel crystal using first-principles calculations. The pressure was found to promote an *interspin* charge transfer, eventually equalizing the charge population between $3d^{\uparrow}$ and $3d^{\downarrow}$ states. The driving force for this charge transfer was discussed to be the enhancement of the crystal-field splitting between the e_g and the t_{2g} bands, enabling the former to form chemical bonds between the NNN Ni ions at the expense of partial depopulations of the latter. These findings shed light on the behavior of complex orbital manifolds subject to strong crystal fields and Coulombic interactions.

ACKNOWLEDGMENTS

M.S.B. gratefully acknowledges the Research Infrastructures at the University of Manchester for allocations on the CSF3 high performance computing facilities. A.A. is grateful to Dr. D. K. Shukla for his encouraging supports.

[1] H.-K. Mao, X.-J. Chen, Y. Ding, B. Li, and L. Wang, Rev. Mod. Phys. **90**, 015007 (2018).
[2] V. Moruzzi and P. Marcus, Phys. Rev. B **38**, 1613 (1988).
[3] I. Sergueev, L. Dubrovinsky, M. Ekholm, O.Y. Vekilova, A. Chumakov, M. Zajac, V. Potapkin, I. Kantor, S. Bornemann, H. Ebert, S.I. Simak, I.A. Abrikosov, and R. Ruffer, Phys. Rev. Lett. **111**, 157601 (2013).
[4] P. Mohn, *Magnetism in the Solid State: An Introduction*, Vol. 134 (Springer Science & Business Media, Berlin, 2006).
[5] V. I. Anisimov, J. Zaanen, and O. K. Andersen, Phys. Rev. B **44**, 943 (1991).
[6] M. Nicol and G. Jura, Science **141**, 1035 (1963).
[7] R. Torchio, A. Monza, F. Baudelet, S. Pascarelli, O. Mathon, E. Pugh, D. Antonangeli, and J. P. Itié, Phys. Rev. B **84**, 060403(R) (2011).
[8] Y. S. Mohammed, Y. Yan, H. Wang, K. Li, and X. Du, J. Magn. Magn. Mater. **322**, 653 (2010).
[9] J. Xie, S. Chen, H. V. Brand, and R. L. Rabie, J. Phys.: Condens. Matter **12**, 8953 (2000).
[10] V. Iota, J.-H. P. Klepeis, C.-S. Yoo, J. Lang, D. Haskel, and G. Srajer, Appl. Phys. Lett. **90**, 042505 (2007).
[11] R. Torchio, Y. Kvashnin, S. Pascarelli, O. Mathon, C. Marini, L. Genovese, P. Bruno, G. Garbarino, A. Dewaele, F. Occelli, and P. Loubeyre, Phys. Rev. Lett. **107**, 237202 (2011).
[12] J. Perdew, K. Burke, and M. Ernzerhof, Phys. Rev. Lett. **77**, 3865 (1996).
[13] P. Giannozzi, S. Baroni, N. Bonini, M. Calandra, R. Car, C. Cavazzoni, D. Ceresoli, G. L. Chiarotti, M. Cococcioni, I. Dabo, *et al.*, J. Phys.: Condens. Matter **21**, 395502 (2009).
[14] M. Černý, J. Pokluda, M. Šob, M. Friák, and P. Šandera, Phys. Rev. B **67**, 035116 (2003).
[15] R. Fletcher, *Practical Methods of Optimization* (Wiley, New York, 2013).
[16] I. Souza, N. Marzari, and D. Vanderbilt, Phys. Rev. B **65**, 035109 (2001).
[17] A. A. Mostofi, J. R. Yates, Y.-S. Lee, I. Souza, D. Vanderbilt, and N. Marzari, Comput. Phys. Commun. **178**, 685 (2008).
[18] R. G. Burns and R. G. Burns, *Mineralogical Applications of Crystal Field Theory* (Cambridge University Press, Cambridge, 1993).
[19] M. S. Dresselhaus, G. Dresselhaus, and A. Jorio, *Group Theory: Application to the Physics of Condensed Matter* (Springer Science & Business Media, Berlin, 2007).
[20] S. Blundell, *Magnetism in Condensed Matter*, in Oxford Master Series in Condensed Matter Physics (Oxford University Press, Oxford, 2001).
[21] T. Jarlborg, Physica C: Superconductivity **385**, 513 (2003).
[22] J. Bekaert, A. Aperis, B. Partoens, P. M. Oppeneer, and M. V. Milošević, Phys. Rev. B **97**, 014503 (2018).
[23] H. J. Xiang, E. J. Kan, S.-H. Wei, M.-H. Whangbo, and X. G. Gong, Phys. Rev. B **84**, 224429 (2011).
[24] I. Yang, S. Y. Savrasov, and G. Kotliar, Phys. Rev. Lett. **87**, 216405 (2001).
[25] M. Donath, Surf. Sci. Rep. **20**, 251 (1994).
[26] V. L. Moruzzi, J. F. Janak, and A. R. Williams, *Calculated Electronic Properties of Metals* (Pergamon Press, New York, 1978).
[27] J. Braun, J. Minár, H. Ebert, M. I. Katsnelson, and A. I. Lichtenstein, Phys. Rev. Lett. **97**, 227601 (2006).
[28] S. Chadov, J. Minár, M. I. Katsnelson, H. Ebert, D. Ködderitzsch, and A. I. Lichtenstein, Europhys. Lett. **82**, 37001 (2008).
[29] A. S. Belozerov, A. A. Katanin, and V. I. Anisimov, J. Phys.: Condens. Matter **33**, 385601 (2021).